A stochastic approach to detect fragmentation epoch from a single fragment orbit determination

Marco Felice Montaruli [a,*], Pierluigi Di Lizia [a], Emiliano Cordelli [b], Hélène Ma [c],
Jan Siminski [d]

[a] *Politecnico di Milano, Department of Aerospace Science and Technology (DAER), Via G. La Masa 34, 20156 Milan, Italy*
[b] *GMV@ESA, Space Debris Office (SDO), European Space Operations Centre (ESA/ESOC), Robert-Bosch-Str. 5, 64293 Darmstadt, Germany*
[c] *RHEA System GmbH@ESA, Space Debris Office (SDO), European Space Operations Centre (ESA/ESOC), Robert-Bosch-Str. 5, 64293 Darmstadt, Germany*
[d] *European Space Agency – European Space Operations Centre (ESA/ESOC), Robert-Bosch-Str. 5, 64293 Darmstadt, Germany*

Abstract

In the last decades, the growing in-orbit population of resident space objects has become one of the main concerns for space agencies and institutions worldwide. In this context, fragmentations further contribute to increase the number of space debris and, operationally, it is fundamental to identify the event epoch as soon as possible, even when just a single fragment orbital state, resulting from an Initial Orbit Determination (IOD) process, is available.

This work illustrates the Fragmentation Epoch Detector (FRED) algorithm, which deals with the problem through a stochastic approach, starting from a single fragment IOD result (expressed through mean state and covariance) and parent ephemeris (assumed as deterministic). The process populates the fragment ephemeris with a multivariate normal distribution and, for each couple sample-parent, the epochs of parent transit through the Minimum Orbital Intersection Distance (MOID) are first computed on a time window and then clustered in time. For each cluster, both the three-dimensional MOID and the three-dimensional relative distance distributions are derived, and their similarity is statistically assessed. Given that, at the actual fragmentation epoch, MOID and relative distance were equal, the cluster featuring the best matching between the two distributions is considered as the optimal candidate, and the related fragmentation epoch is returned from the time of parent transit through the MOID, in terms of mean and standard deviation.

FRED algorithm performance is assessed through a numerical analysis. The algorithm robustness decreases when parent and fragment orbits share a similar geometry, and results get deteriorated if the perturbations and, moreover, the IOD errors are included in the process, but the correct fragmentation epoch is always present among candidates. Overall, FRED algorithm turns out to be a valid choice in operational scenarios, and a sensitivity analysis tests the algorithm out of the nominal conditions.

1. Introduction

In the last decades, the number of man-made objects orbiting the Earth has dramatically increased. In around 65 years of space activities, more than 6340 successful launches have taken place, which turned out in about 14710 objects placed in Earth orbit (ESA, 2023). Among

* Corresponding author.

E-mail addresses: marcofelice.montaruli@polimi.it (M.F. Montaruli), pierluigi.dilizia@polimi.it (P. Di Lizia), emiliano.cordelli@ext.esa.int (E. Cordelli), helene.ma@ext.esa.int (H. Ma), jan.siminski@esa.int (J. Siminski).

these, 9780 are still orbiting, but only 7000 are active. In addition, about 640 break-ups, explosions, collisions, or anomalous events resulting in fragmentation have been recorded, which have further contributed to the increase in the orbiting population of man-made objects. In this context, space debris are considered as all the artificial objects including fragments and elements thereof, in Earth orbit or re-entering the atmosphere, that are non functional (IADC, 2002). Nowadays, 32500 debris objects are regularly tracked by space surveillance networks and maintained in their catalogue (ESA, 2023). In addition to them, statistical models estimate that there are 36500 objects greater than 10 cm, one million objects between 1 cm and 10 cm, and 130 million objects between 1 mm and 1 cm. Their presence may jeopardise the operative mission of active satellites, given that the possible impact with a space debris ranges from cumulative erosion of satellite surface, for debris smaller than 0.1 mm, to the possible satellite destruction, with the generation of thousands of additional pieces of debris and inevitable environmental drawbacks and possible cascade effects (Kessler and Cour-Palais, 1978).

To mitigate mission-related risks, specific Space Surveillance and Tracking (SST) programs were started to build the expertise required to manage the challenges posed by the Space Traffic Management (STM). To prevent the above-mentioned proliferation of space debris, particular attention is devoted to fragmentation events, which may further contribute to increase the number of space debris objects (McKnight et al., 2021). Therefore, it is fundamental to apply models predicting the fragments cloud evolution, like the ones in (Letizia et al., 2015 and Letizia et al., 2016), in order to assess possible collisions, and, for this purpose, the time when the break-up occurred shall be identified to set the proper initial conditions.

In Andrisan et al. (2016) the fragmentation epoch is evaluated as the point of minimum distance of all the fragments with respect to the cloud centre of mass. In Frey et al. (2018) the break-up epoch is determined by detecting a convergence of fragments in the space of inclination and right ascension of the ascending node. In Di Mare et al. (2019) a critical study is conducted to identify the best criterion to assess the event epoch from the fragments ephemerides, and a sensitivity analysis on the cloud orbital position is conducted. In Romano et al. (2021) a process is proposed, which screens a catalogue of ephemerides, detects possible break-ups of satellites and identifies those related to fragments, through the filters presented in Hoots et al. (1984). After the filtering phase, the same criteria are applied combined with SGP4 propagation (Vallado et al., 2006) and, by comparing the algorithm outputs among all the fragments, the fragmentation epoch is identified. All these works need many fragments ephemerides, and use them as a deterministic information.

The numerous accurate ephemerides availability of the space debris originated by the fragmentation event is a quite optimistic assumption, as, from an operational point of view, it could be necessary to estimate the fragmentation epoch just few hours after the event, and very few ephemerides (even only one) could be available. Indeed, it may take days and even months to have a large number of ephemerides. In addition, when a fragments cloud is observed, the correlation of measurements to a single fragment is a very challenging task, and this further decreases the number of ephemerides which can be used in a reliable way. Next, such ephemerides could be inaccurate, because of the noise of the observation measurements and the error introduced by the Initial Orbit Determination (IOD) algorithm exploited, and their uncertainty cannot be neglected during the event characterisation. Nevertheless, a prompt knowledge of the fragmentation epoch would be fundamental to plan additional observations of the fragments cloud, e.g. by tasking the sensors to point at the right ascension and declination where the parent was when broke up. Indeed, all the fragments are expected to transit close to that inertial region in the first hours after the event, before that their orbit modification due to orbital perturbations becomes too relevant. Also, knowing the fragmentation epoch would allow to model the break-up event, which may be used to task sensors for early detection. In addition, the knowledge of the fragmentation epoch would be important to refine the processing of the observation measurements, aiming at obtaining more and more accurate orbit determination results. This would lead to also refine the estimation of the fragmentation epoch and, so, a virtuous cycle would be generated.

The aim of the present work is to provide an operational procedure to estimate the fragmentation epoch starting from the last available ephemeris of the parent object (assumed as a deterministic quantity) and a single fragment orbital state provided with uncertainty. The latter is considered as determined, in the hours right after the fragmentation alert, by a IOD process from a single observation with no transit prediction. Such an approach would support operators to characterise fragmentations when a satellite break-up is detected and a measurements track (sufficient to provide an orbit determination result) is acquired few hours later, and it is associated to the event..

To accomplish the purpose of the work, the FRagmentation Epoch Detector (FRED) algorithm, implementing a stochastic approach, is described in Section 2 and its performance are assessed in Section 3 through numerical simulations.————————————————————

2. FRagmentation Epoch Detector - FRED

Let's consider the fragmentation of a space object whose last available ephemeris x^p is dated to t_{eph}, and is considered as a deterministic information. The event has occurred at $t_0 > t_{eph}$ and the related alert has been notified at $t_a > t_0$. Some hours later, one fragment is detected by an on-ground sensor at t_{obs} (with $t_{obs} > t_a$) and its orbital state

$\{\boldsymbol{x}^{fg}, \boldsymbol{P}^{fg}\}$ is first determined, where the mean $\boldsymbol{x}^{fg}$ and covariance $\boldsymbol{P}^{fg}$ are directly derived from the IOD process.

If the orbit determination were very accurate and both the physical parameters and the dynamical model were well known, it would be theoretically possible to propagate both the fragment and the parent object in the time window $[t_{eph}, t_a]$ and search for the epoch of the minimum relative distance, which would correspond to the fragmentation epoch t_0. However, in real applications, both the measurements accuracy and the IOD process introduce an error in the reconstruction of the observed fragment state vector, and the above-mentioned method turns out to be unreliable. As an example, Fig. 1 represents the relative distance trend on an analysis time window between the parent object last available ephemeris and an observed fragment mean state to which an IOD error of 1.85e-02 km in position and 4.99e-04 km/s in velocity is attributed (continuous line). Such an error is retrieved from a synthetic IOD process based on the method presented in (Siminski, 2016) and starting from angular track and slant range to which Gaussian noises of 0.01 deg and 30 m are added, respectively. It can be observed that the epoch of the minimum relative distance between fragment and parent mean states (dashed dense line) is completely different from the correct fragmentation epoch (dashed line), that is the epoch corresponding to the theoretical minimum relative distance (dashed black line). A further source of error is represented by the mismatching between the actual fragment trajectory and the propagation model used, due, for

instance, to the fact that the actual physical parameters of the observed fragment are not known. For all these reasons, assessing the fragmentation epoch by just searching for the minimum relative distance between $\boldsymbol{x}^p$ and $\boldsymbol{x}^{fg}$ in the time window $[t_{eph}, t_a]$ is an unreliable methodology.

The considerations above imply that the orbit determination uncertainty cannot be a priori neglected. For this reason FRED algorithm deals with the fragmentation epoch identification problem through a stochastic approach, starting from a Monte Carlo distribution of the orbit determination result. Ideally, at the fragmentation epoch, both the Minimum Orbital Intersection Distance (MOID) (Gronchi, 2005) and the relative distance between the parent and the fragment are expected to be zero. Due to the considerations above, in practical cases neither MOID nor relative distance turn out to be null, but they should statistically match each other. Therefore, the correct fragmentation epoch is expected to feature a matching between the MOID and the relative distance distributions.

FRED algorithm flowchart is reported in Fig. 2, and is structured as follows.

1. In order to include the fragment state uncertainty in the event epoch identification, N_s samples $\boldsymbol{x}^s$ are generated from the orbital state $\{\boldsymbol{x}^{fg}, \boldsymbol{P}^{fg}\}$ according to a multi-normal distribution (Kotz et al., 2000). The parameter N_s can be selected by the user to guarantee a trade-off between a proper uncertainty sampling and the computational demand of the algorithm (which is directly proportional to the number of samples used).

2. The time window $[t_{eph}, t_a]$ is sampled with frequency $1/T^p$ (where T^p is the parent orbital period). This results in the epochs t_i, whose number is n_{orb}.

3. Both parent and fragment samples orbital states are propagated to each t_i.

4. For each t_i and for each j-th fragment sample, the epochs of transit through the MOID of both the parent and the fragment j-th sample are computed analytically, according to (Gronchi, 2005), and indicated as t_j^p and t_j^s. The parent and the j-th sample state vectors are propagated up to t_j^p and t_j^s respectively, resulting in the orbital states $\boldsymbol{x}^p(t_j^p)$ and $\boldsymbol{x}^s(t_j^s)$, and the analytical computations of t_j^p and t_j^s are updated. The epochs t_j^p and t_j^s are iteratively modified in this manner until, between two consecutive steps, they do not change anymore (according to a tolerance set equal to 1e-03 s). This iterative process results in $N_s \times n_{orb}$ couples of $\left(t_j^p, t_j^s\right)$ and $\left(\boldsymbol{x}^p(t_j^p), \boldsymbol{x}^s(t_j^s)\right)$. It is important to observe that the difference between $\boldsymbol{p}^s(t_j^s)$ and $\boldsymbol{p}^p(t_j^p)$ (the $\boldsymbol{x}^s(t_j^s)$ and $\boldsymbol{x}^p(t_j^p)$ positions) allows to compute the MOID (usually described in a scalar way (Gronchi, 2005)) in 3 dimensions: $\boldsymbol{m}_j = \boldsymbol{p}^s(t_j^s) - \boldsymbol{p}^p(t_j^p)$.
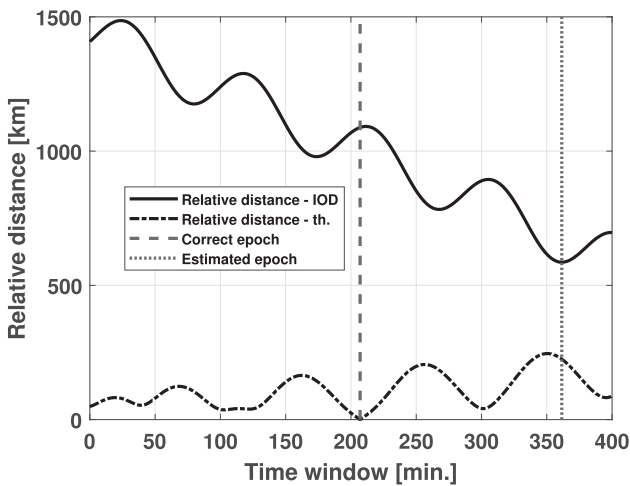

Fig. 1. Relative distance between the parent object and the mean state of one observed fragment. Their state vectors are propagated on a time window ranging from the last available ephemeris of the parent object to the event alert. The dashed curve line shows the theoretical trend and the dashed straight line corresponds to the epoch of minimum value, that is the fragmentation epoch. On the contrary, the continuous black line shows the relative distance trend when an IOD error is attributed to the fragment mean state, and the dashed dense line corresponds to the minimum value, that is the estimated fragmentation epoch. It is possible to see that the estimated fragmentation epoch is completely different from the correct value.
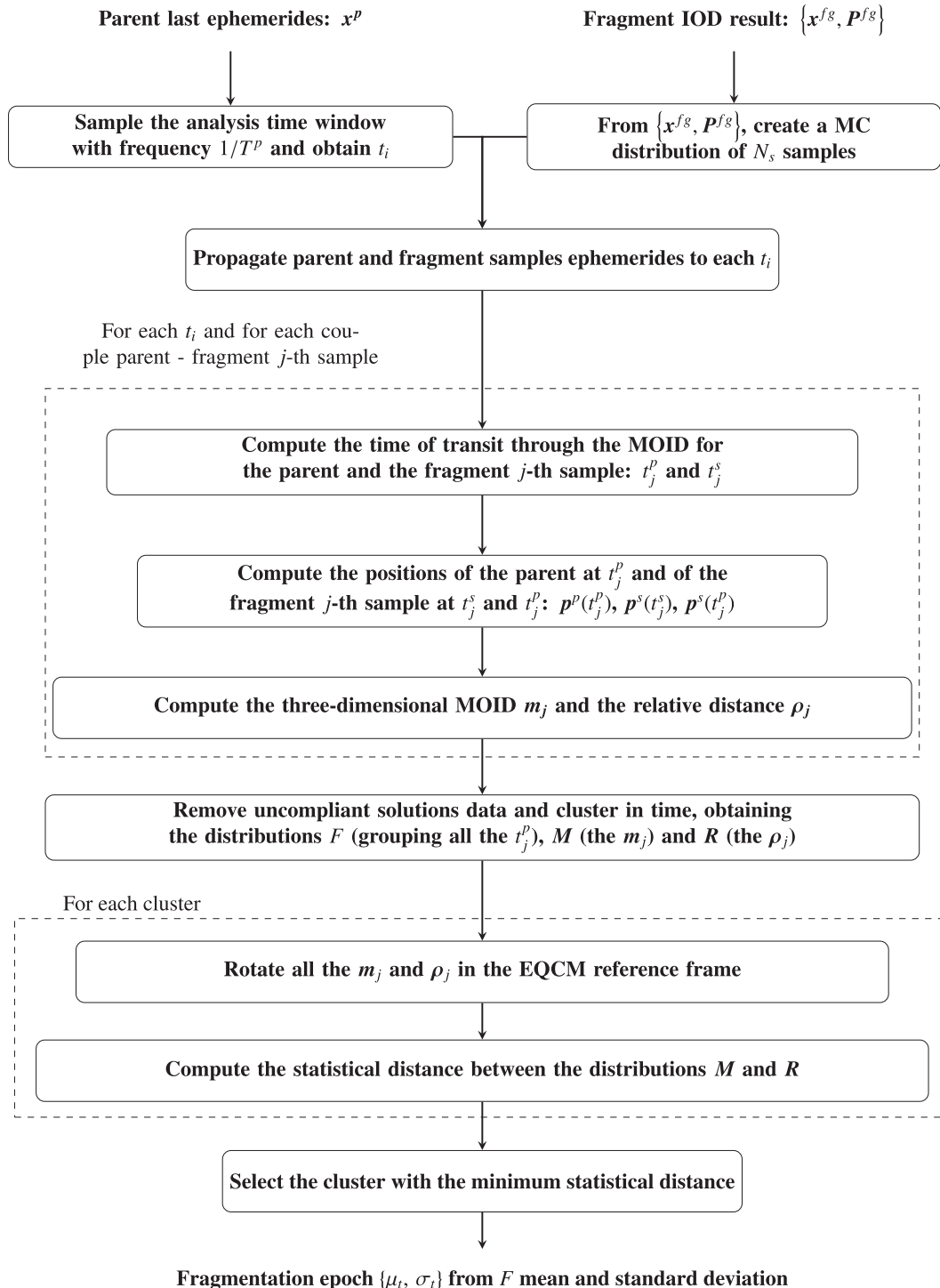
Parent last ephemerides: x^p

Fragment IOD result: $\{x^{fg}, P^{fg}\}$

Sample the analysis time window
with frequency $1/T^p$ and obtain t_i

From $\{x^{fg}, P^{fg}\}$, create a MC
distribution of N_s samples

Propagate parent and fragment samples ephemerides to each t_i

For each t_i and for each cou-
ple parent - fragment j-th sample

Compute the time of transit through the MOID for
the parent and the fragment j-th sample: t_j^p and t_j^s

Compute the positions of the parent at t_j^p and of the
fragment j-th sample at t_j^s and t_j^p: $p^p(t_j^p)$, $p^s(t_j^s)$, $p^s(t_j^p)$

Compute the three-dimensional MOID m_j and the relative distance ρ_j

Remove uncompliant solutions data and cluster in time, obtaining
the distributions F (grouping all the t_j^p), M (the m_j) and R (the ρ_j)

For each cluster

Rotate all the m_j and ρ_j in the EQCM reference frame

Compute the statistical distance between the distributions M and R

Select the cluster with the minimum statistical distance

Fragmentation epoch $\{\mu_t, \sigma_t\}$ from F mean and standard deviation

Fig. 2. FRED algorithm flowchart.

5. The fragment j-th sample state vector $x^s(t_j^s)$ is propagated up to the epoch of parent transit through the MOID, resulting in $x^s(t_j^p)$. It is worth to observe that the difference between the $p^s(t_j^p)$ (the $x^s(t_j^p)$ position) and $p^p(t_j^p)$ provides the three-dimensional relative distance between the j-th sample and the parent, at the epoch of parent transit through the MOID:

$\rho_j = p^s(t_j^p) - p^p(t_j^p)$. Fig. 3 provides a two-dimensional sketch of the parent and fragment sample orbits, with the involved quantities.

6. To exclude unfeasible solutions, the $N_s \times n_{orb}$ couples enter a filtering phase, which is based on the epoch of parent transit through the MOID t_j^p. Being related to the parent ephemeris, that is the information considered more reliable (and so assumed as deterministic),
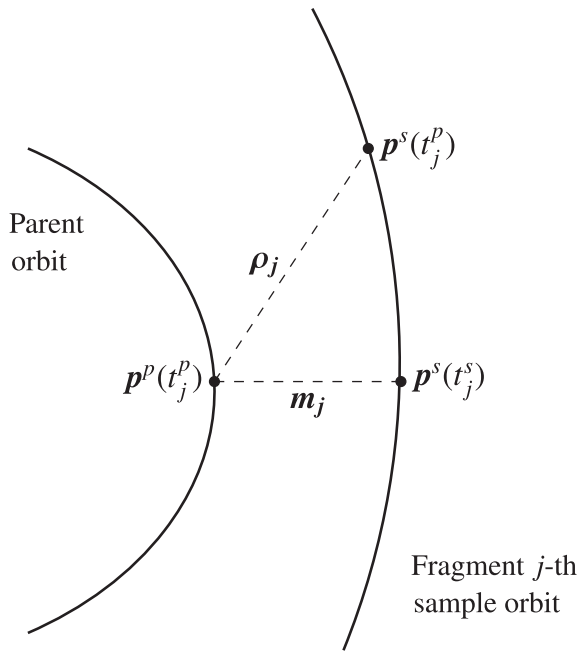
Fig. 3. Sketch of the parent and fragment sample orbits, with the quantities involved in FRED algorithm process.

it is selected instead of the time of the fragment j-th sample transit through the MOID t_j^s. The filtering phase is structured as follows:

(a) First, the couples for which t_j^p is not included in the boundaries $[t_{eph}, t_a]$ are filtered out.

(b) Then, the couples computed from the state vectors propagated at epoch t_i and for which $t_j^p < (t_i - T^p/2)$ or $t_j^p > (t_i + T^p/2)$ are removed from the data set. This operation is done because the MOID data $\left(t_j^p, t_j^s, \boldsymbol{p}^p(t_j^p), \boldsymbol{p}^s(t_j^s), \boldsymbol{p}^s(t_j^p)\right)$ are computed for each periodicity. Thus, if t_j^p is computed from orbital states at t_i, it must belong to the i-th periodicity, that is the time difference $|t_i - t_j^p|$ shall be smaller than half of the parent orbital period T^p.

7. All the remaining n_{filter} epochs t_j^p are clustered according to a Density-Based Spatial Clustering of Applications with Noise (DBSCAN) (Ester et al., 1996). From this operation, n_{orb} are expected to be identified. However, for those situations in which parent and fragment orbits are similar (especially in inclination and right ascension of the ascending node), multiple clusters are possibly identified for each i-th periodicity, as the epochs t_j^p change significantly from a j-th sample to another one. So, more generally, n_{cl} clusters are considered to be identified. Fig. 4a presents the obtained clusters, in the plane t_j^p (in Coordinated Universal Time, UTC) versus scalar MOID. It

is worth to remark that the MOID values are equal from a periodicity to the other, as the graph is related to a Keplerian scenario, in which, for a single parent j-th sample couple, the MOID does not change.

8. For each n-th cluster, the candidate fragmentation epoch t_n^{fg} can be computed (in terms of mean and standard deviation) from the distribution of the epoch of parent transit through the MOID, which is indicated as F, and which is represented in Fig. 4b (for the correct cluster). In addition, $\boldsymbol{M}$ and $\boldsymbol{R}$ distributions (grouping the $\boldsymbol{m}_j$ and $\boldsymbol{\rho}_j$ respectively) are associated to each cluster. Fig. 5 shows the two distributions in Earth-Central-Inertial (ECI) reference frame, both for the correct candidate and for a non-correct one. It is possible to observe that the three-dimensional MOID distribution $\boldsymbol{M}$ is much more concentrated than the relative distance one $\boldsymbol{R}$. This is due to the fact that, from sample to sample, the change in t_j^p causes a remarkable modification in the relative distance $\boldsymbol{\rho}_j$ (as it is time-dependent), but not in the MOID $\boldsymbol{m}_j$, which is the geometrical difference between the parent and the j-th sample orbits and, so, does not vary remarkably from a sample to another.

9. Afterwards, for each cluster:

(a) All the $\boldsymbol{m}_j$ and $\boldsymbol{\rho}_j$ are rotated in the Modified Equidistant Cylindrical (EQCM) reference frame (Vallado and Alfano, 2014). This operation results in MOID and relative distance distributions like in Fig. 6. The MOID distribution $\boldsymbol{M}$ is almost two-dimensional, as, in all the $\boldsymbol{m}_j$, the y-component, expressing the along orbit curvature relative distance, is negligible.

(b) The statistical distance between $\boldsymbol{M}$ and $\boldsymbol{R}$ distributions is computed according to one of the metrics discussed below.

10. Repeating the operations above for each cluster results in Fig. 7, which shows the statistical distance computed through the Earth Mover's Distance (EMD) (Levina and Bickel, 2001) (discussed below) in function of the F distribution mean. Finally, the cluster featuring the minimum statistical distance between the $\boldsymbol{M}$ and $\boldsymbol{R}$ distributions is selected, and the fragmentation epoch is returned from the related distribution F, in terms of mean μ_t and standard deviation σ_t.

As mentioned above, this process provides a pattern to derive the fragmentation epoch (in terms of mean and standard deviation) through a stochastic approach, starting from the last available parent ephemeris and the fragment IOD result. However, there are two theoretical sources of failure:
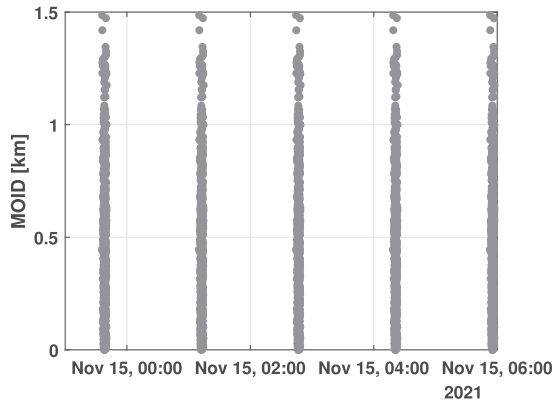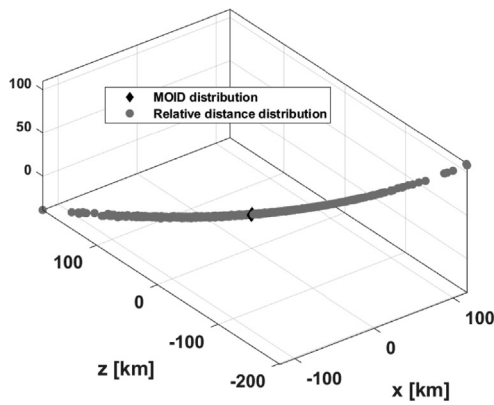
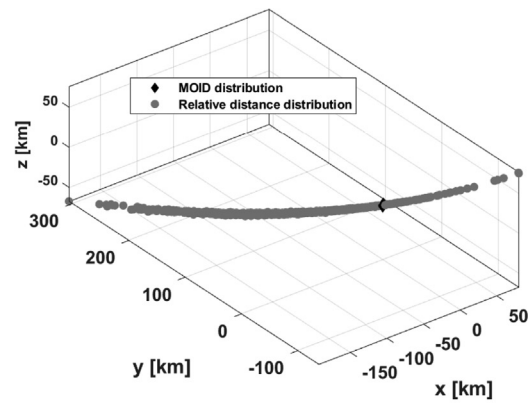(a) Distribution of the t_j^p epochs in the time window of the analysis.
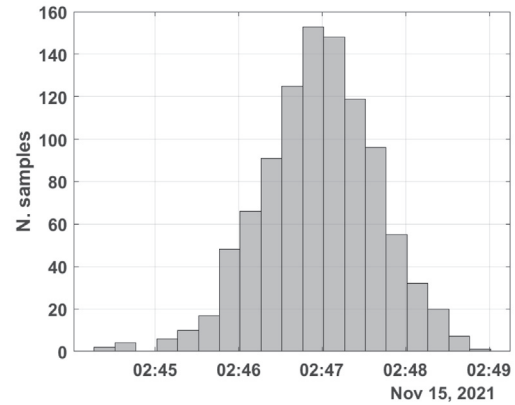
(b) Distribution of the t_j^p epochs for the cluster related to the correct solution.

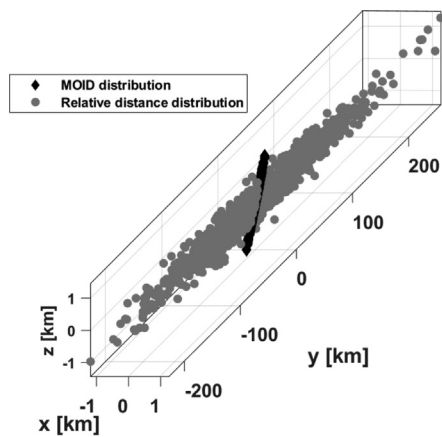Fig. 4. Results of the clustering phase. The epochs are reported in UTC.
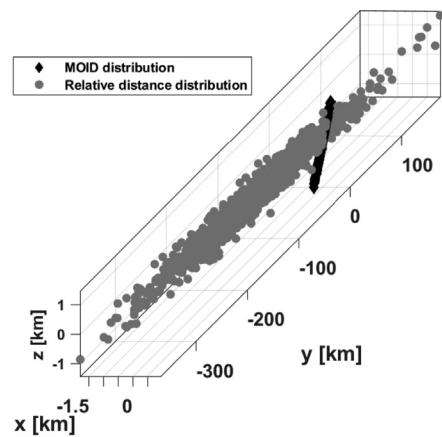

(a) Cluster related to the correct epoch.

(b) Cluster related to a wrong epoch.

Fig. 5. M and R distributions in ECI reference frame, for the correct cluster and a non-correct one.

(a) Cluster related to the correct epoch.

(b) Cluster related to a wrong epoch.

Fig. 6. M and R distributions in EQCM reference frame, for the correct cluster and a non-correct one.
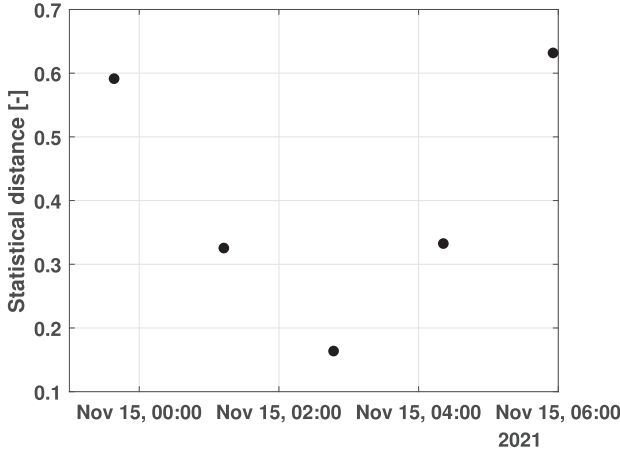
Fig. 7. EMD statistical distance computed for each cluster.

- The MOID computation turns out to be very sensitive when the orbital planes of the fragment and parent orbits are very close each other (that is, they have similar inclination and right ascension of the ascending node). In this case, the change in the fragment orbit, occurring from sample to sample, may provoke a remarkable variation in the MOID data computation. As result, F distribution expand, and, for the correct candidate, it may not cluster around the actual fragmentation epoch, but around an epoch distant up to tens of minutes.
- The relative distance distribution R does not change from a cluster to another when the fragment and parent orbital periods are very close each other (that is, they have similar semi-major axis). In this case, for a j-th sample, from a i-th periodicity to the following one, the relative distance ρ_j does not change significantly. As result, it is not straightforward to recognise the correct cluster from the statistical distance metrics, and the wrong fragmentation epoch is possibly returned by the process.

As introduced above, FRED needs a statistical distance metrics to assess the best epoch candidate. Expressing M and R distributions through their mean and covariance as $\{\boldsymbol{\mu_M}, \boldsymbol{P_M}\}$ and $\{\boldsymbol{\mu_R}, \boldsymbol{P_R}\}$ respectively, a possible choice is represented by the Mahalanobis Distance (Mahalanobis, 1936):

$$\xi = \sqrt{\{\boldsymbol{\mu_M} - \boldsymbol{\mu_R}\}^T \{\boldsymbol{P_M} + \boldsymbol{P_R}\}^{-1} \{\boldsymbol{\mu_M} - \boldsymbol{\mu_R}\}} \qquad (1)$$

However such a metrics applies to Gaussian distributions only. Even if supported by the rotation to EQCM reference frame, assuming Gaussian distributions would be a particularly strong assumption for M and R distributions. To be as generic and agnostic as possible regarding the distributions characteristics, metrics suitable both for Gaussian and no Gaussian distributions are investigated.

A first choice is represented by the Earth Mover's Distance (EMD) (Levina and Bickel, 2001), which measures

the flow to pass from a distribution to the other one. Such a flow can be evaluated based on different distance metrics, and the Euclidean distance weighted on the distribution variance is chosen to better account for M and R distributions shape and elongation. The implementation provided in (SciPy, 2022) is used.

A third metrics is investigated, which has been developed specifically for FRED algorithm. It is addressed as the *quantile* metrics given its workflow, which is described as follows.

1. For both M and R distributions a Principal Component Analysis (PCA) is performed to rotate them in their respective principal coordinate reference frame (Jolliffe, 2011). Then, for each distribution, the quantiles 10%, 25%, 50%, 75% and 90% are computed for the three coordinates separately. This operation does not account for the correlations among coordinates, but these have been minimised thanks to the rotation to the principal coordinate reference frame. This results in two sequences (for M and R) of three-dimensional points, expressed in two different principal coordinate reference frames.
2. The two sequences of three-dimensional points (expressing the quantiles) are rotated back to the original EQCM reference frame, in order to have them in a common coordinate system. Fig. 8 shows the two sequences of three-dimensional points, for the correct and for a wrong epoch. Then, the five quantile-to-quantile Euclidean distances are computed and summed together in a weighted manner according to the quantile percentage (that is, by advantaging more the central quantiles with respect to the side ones). This weighted sum provides the statistical distance which accounts for the similarity between the two non-Gaussian distributions M and R.

A critical comparison among the metrics presented above is proposed during the numerical analysis in Section 3.2.

Analogies and differences with conjunction analysis

From the FRED description, the reader may easily notice that dealing with the fragmentation detection problem in such a stochastic way presents analogies with the conjunction analysis. In particular, the process involves the MOID and the relative distance, which are quantities usually exploited also in the screening part of the conjunction assessment (Hoots et al., 1984), as well as in other fragmentation epoch identification algorithms (like in (Di Mare et al., 2019 and Romano et al., 2021)) which use the availability of many fragments orbital states, then processed in a deterministic way. However, at this level a first difference arises. Indeed, in FRED, the screening is fully stochastic and is only based on the time of parent transit through the MOID. In addition, the FRED screening phase does not aim at identifying possible conjunctions,
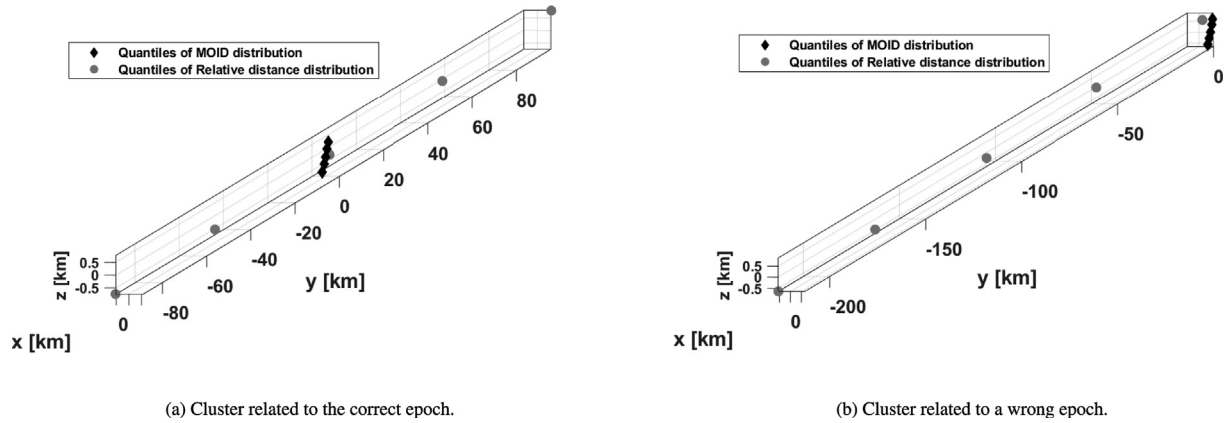
(a) Cluster related to the correct epoch.

(b) Cluster related to a wrong epoch.

Fig. 8. Quantile sequences for M and R distributions in EQCM reference frame.

as the fragmentation is already known to have occurred, but to rank conjunction (that is fragmentation epoch) candidates. Thus, the MOID and the relative distance are not quantities used to search for a possible conjunction in a deterministic way, but they are stochastically represented at the fragmentation epoch candidates, and then their statistical distance is computed.

At this point, a second analogy may be noticed, as in both cases a stochastic quantity is expressed at the time of closest approach: the Probability of Collision (PoC) in the conjunction analysis and the statistical distance between MOID and relative distance distributions in FRED. However, besides the two metrics differently defined, a remarkable difference arises: while in conjunction analysis the PoC is a quantity assessing the danger associated to a single conjunction and, so, expressing an absolute meaning, in FRED the statistical distance is used to rank the fragmentation epoch candidates previously identified, and so it has a relative meaning.

3. Numerical simulations

3.1. Data set generation

A numerical simulation is here conducted to test FRED algorithm. The fragmentation scenario is the one which involved the Russian satellite COSMOS 1408 during the kinetic anti-satellite (ASAT) test which occurred around 02:47 UTC of November 15th, 2021 (EUSST, 2021). The ASAT test took place when the satellite was flying over the north-west Russia and the sensors of the EUSST consortium (European Space Surveillance and Tracking, 2021) observed the fragments generated by such an event.

The data set to test FRED algorithm is generated as follows:

1. The last available COSMOS 1408 ephemeris before the event are retrieved from the last TLE (Two-Line Elements) available on Spacetrack, which are dated to 00:55 UTC of November 15th (Space-track, 2022);

(Hoots and Roehrich, 1980). To make the analysis time window more symmetrical with respect to the break-up epoch, they are propagated one orbital period back to the 23:20 UTC of November 14th, and the orbital state at this epoch is considered as x^p. This operation has been taken to assess algorithm behaviour when the fragmentation epoch candidates distribution is as symmetric as possible with respect to the correct epoch.

2. The state vector x^p is propagated up to 02:47:00 UTC of November 15th. Table 1 reports COSMOS 1408 orbital parameters, simulated at the fragmentation epoch.

3. The fragmentation event is modelled as a set of impulses applied to the satellite orbital state at 02:47:00 UTC. These impulses, generating one single fragment each, are retrieved from the NASA standard break-up model (NASA, 2011). By this way, a data set of 231 fragments is created by setting the parent object mass equal to 200 kg and the fragments characteristic length ranging from 0.01 m to 2.1 m. These values were selected to obtain a manageable and complete impulse data set size rather than to model the event in a realistic way. The simulated fragments cloud characteristics are described in Fig. 9, both in terms of impulse magnitude distribution of the fragmentation event and Gabbard diagram.

The obtained ephemerides, representing the fragments, are propagated until the epoch t_{obs}, when they are detected by an on-ground sensor, and the orbital states $\{x^{fg}, P^{fg}\}$ are determined. The propagation model used depends on the analysis conducted, as detailed throughout the rest of Section 3.

Table 1
COSMOS 1408 orbital parameters simulated on November 15th 2022, at 02:47:00 UTC.

a [km]	e	i [deg]	Ω [deg]	ω [deg]	θ [deg]
6862.2	2.9e-03	82.7	123.4	91.9	341.8

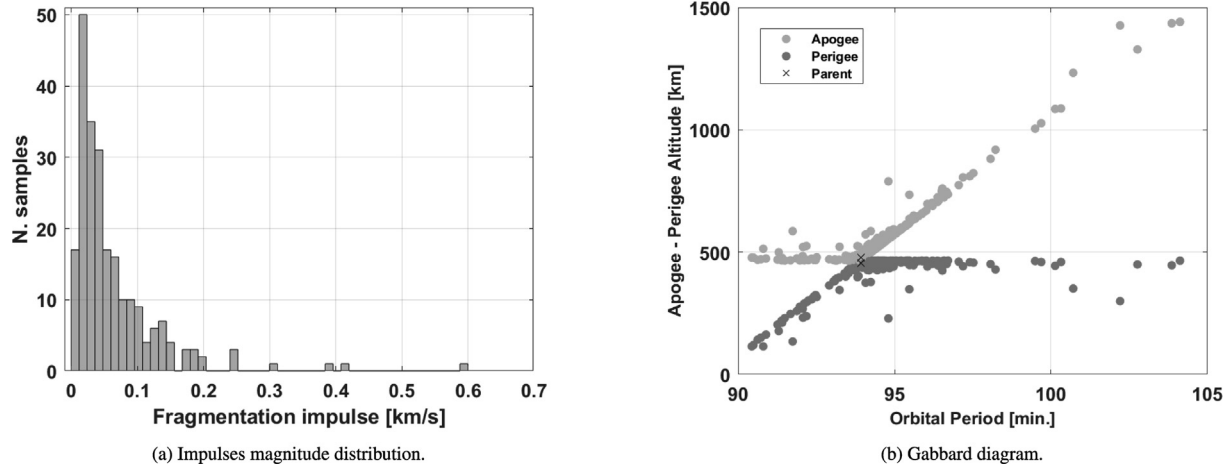(a) Impulses magnitude distribution.

(b) Gabbard diagram.

Fig. 9. Fragmentation event.

In this way all the inputs for the process described in Section 2 are obtained, and FRED algorithm can be tested, considering an analysis time window ranging from 23:20 UTC of November 14th (epoch of the simulated last available ephemeris of the parent object) to 06:00 UTC of November 15th, retracing the fact that the COSMOS 1408 fragmentation alert was provided in the early morning (considering UTC time coordinates). These two epochs correspond to t_{eph} and t_a introduced in Section 2. Instead, the t_{obs} changes from an analysis to the other, as discussed below.

Based on this data set, FRED is run on each fragment IOD result $\{x^{fg}, P^{fg}\}$ separately, considering $N_s=1\mathrm{e}+03$ samples for the multi-normal distribution.

3.2. Unperturbed scenario with no IOD error

First, the unperturbed scenario, considering a two-body dynamics and with no IOD orbital state error is tested to assess the theoretical characteristics of FRED algorithm in ideal conditions. For this purpose, an analytic propagator with no orbital perturbations is exploited. This simulation just associates a covariance P^{fg} (with standard deviations 2.6e-02 km and 7.0e-04 km/s, for inertial position and velocity respectively, computed simulating an IOD with the method presented in (Siminski, 2016)) to the nominal value x^{fg}, that is the fragments propagated state vectors. Thus, the fragment mean state μ^{fg} is the actual fragment position and velocity at t_{obs}. The parent last available ephemeris x^p is the same used above to generate the fragmentation, and the observation epoch t_{obs} is set 13 h after the event, as the method aims at reconstructing the fragmentation epoch from a single fragment observation conducted in the hours right after the event.

For a single fragment analysis, the result is considered successful if the difference between the epoch estimation and the correct value (t_{err}) is below a threshold quantity, which is set equal to 1 min in the analysis, coherently with the time uncertainty associated to the estimated fragmenta-

tion epoch in (Muciaccia et al., 2022). As introduced in Section 2, possible FRED failures can be linked to either the MOID computation or to the distributions comparison performed through the statistical metrics, and for this reason they are classified as follows:

- MOID failures - compliant: $1\ \mathrm{min} < t_{err}$ and $t_{err} < 3\sigma_t$. These are cases for which the fragment orbit orientation is so similar to the parent one that a slight change in the fragment orbit, occurring from fragment mean state to its samples, causes a remarkable variation in the MOID data computation. This leads to an erroneous estimation of the mean epoch of parent transit through the MOID, but the distribution is wide enough to include such an error. Therefore, the resulting epoch estimation is wrong, but statistically compliant.
- MOID failures - uncompliant: $1\ \mathrm{min} < t_{err}$ and $3\sigma_t < t_{err} < T^p/2$. In these cases, the erroneous estimation of the epoch is not mitigated by its uncertainty. The epoch estimation is wrong, but the error is smaller than the half of the parent orbital period.
- Periodicity failures: $t_{err} > T^p/2$. In these cases, the statistical comparison among clusters identifies a wrong candidate and, so, a wrong result is returned. It is worth to remark that MOID failures may occur also when a wrong candidate is identified. Nevertheless, also this situation is addressed as a periodicity failure, as the time error is anyways larger than half of the parent orbital period.

The results are reported on Table 2, for each statistical distance metrics introduced in Section 2. It can be observed that all the metrics feature comparable results, but the EMD ones are the most appreciable.

An analysis is also conducted to assess the Gaussianity of the problem, in order to evaluate whether the Mahalanobis Distance metrics, which needs the Gaussian assumption of the involved distributions, is a suitable choice. For each fragment, the Mahalanobis Distances between each ρ_j and each m_j and the distributions R and

Table 2
Unperturbed scenario results for the different statistical distance metrics.

Metrics	Correct solutions	MOID failures compliant	MOID failures uncompliant	Periodicity failures
Mahalanobis Distance	91.1%	4.2%	1.3%	3.4%
EMD	92.8%	4.7%	0.4%	2.1%
Quantiles	89.5%	4.2%	0.8%	5.5%

(a) MOID distribution.

(b) Focus on the MOID distribution.

(c) Relative distance distribution.

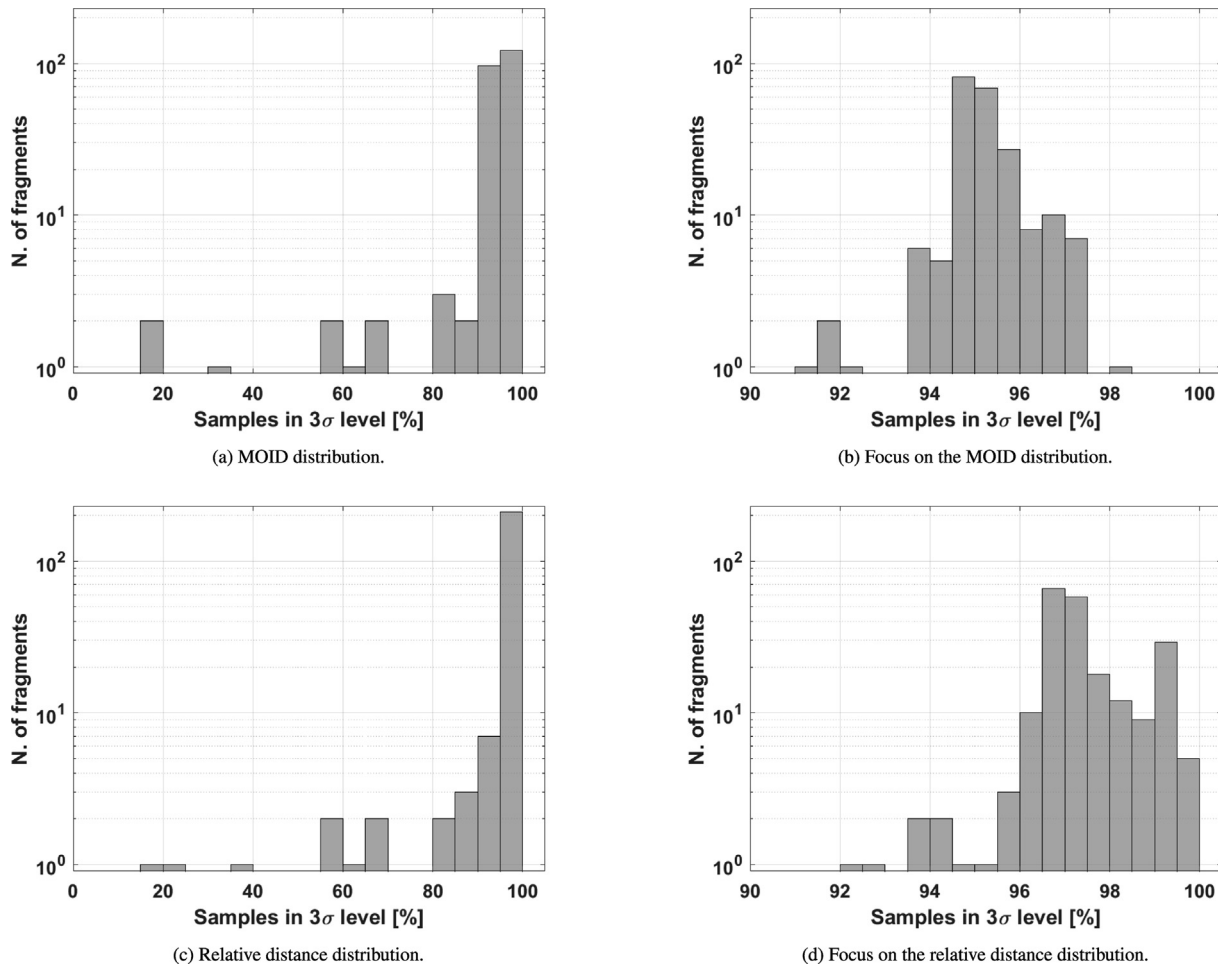(d) Focus on the relative distance distribution.

Fig. 10. Number of fragments (in logarithmic scale) in function of the mean percentage of samples (across the clusters) satisfying the 3σ level, both for the MOID distribution M and for the relative distance distribution R, by also focusing on the portion of the diagram closest to the expected value of 99%.

M respectively is computed, and a χ^2 test is conducted to check how many Mahalanobis Distances are smaller than the 3σ level, for all the n_{cl} clusters. To fulfil the Gaussian assumption, this condition shall be matched in the 99% of cases. Fig. 10 shows the number of fragments (in logarithmic scale) in function of the mean percentage of samples (across the clusters) satisfying the 3σ level, both for the MOID distribution M and for the relative distance distribution R, by also focusing on the portion of the diagram closest to the expected value of 99%. It can be observed that no fragment satisfies the 99% requirement in the MOID distribution M, with lot of cases showing a low percentage of samples within the 3σ level. For some fragments the relative distance distribution R features Gaussianity, but the 99% requirement is not fulfilled in most cases.

This analysis proves that a non-Gaussian metrics shall be considered and, so, the Mahalanobis Distance is rejected. Furthermore, given the results in Table 2, the Earth Mover Distance metrics is selected, as it features the best performance. Therefore, next analyses always apply EMD to identify the best epoch candidates.

EMD results and failures assessment
Fig. 11 shows, for each fragment analysed, the relationship between the magnitude of the impulse which generated it (in logarithmic scale) and the time error between the estimated and the correct fragmentation epochs. It is possible to notice that, over the 231 fragments analysed, 12 MOID failures occur, out of which 11 are compliant and 1 is not. Then, 5 periodicity failures are present, and they are cases
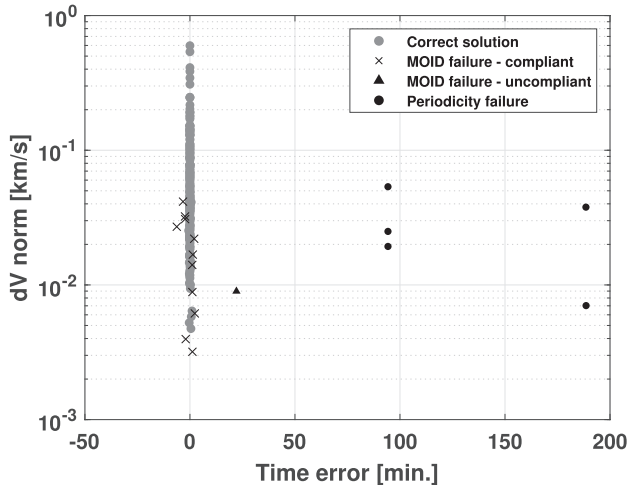
Fig. 11. Results of the numerical analysis on the unperturbed scenario with no orbital state error, by using the EMD metrics. The graph represents, for each fragment analysed, the relationship between the magnitude of the impulse which generated it (in logarithmic scale) and the time error between the estimated and the correct fragmentation epochs. The fragments for which a failure occurs are highlighted according to the legend.

for which the EMD metrics returns similar values across the candidates, among which the correct solution is always present, and the process returns a wrong epoch. It may be noticed that, as general trend, the larger the impulse, the more robust FRED algorithm is. Indeed, a fragment originated by a large impulse magnitude is expected to feature an orbit remarkably different from the parent one both in terms of orbital plane (inclination and right ascension of the ascending node) and of shape (semi-major axis and eccentricity). Thus, it does not run into the theoretical failure sources mentioned in Section 1.

To further assess the problem, it is useful to relate the time standard deviation of the computed fragmentation epoch to the difference between parent and fragments orbital parameters, as represented in Fig. 12. The closer the fragment orbit to the parent one, the larger the time standard deviation associated to the FRED solution, especially for what concerns the inclination and the right ascension of the ascending node (Fig. 12c and Fig. 12d respectively). This behaviour is linked to the fact that the closer the fragment orbit orientation to the parent one, the larger the excursion of the MOID data from a sample to another (as commented in Section 2) and, so, the larger the uncertainty of the time of parent transit through the MOID, that is of the fragmentation epoch candidates. On the contrary, the smallest time uncertainty is related to those fragments with an orbit significantly different from the parent one, as the MOID data do not vary much from a sample to another. Focusing on the the failures characteristics, from Fig. 12a and Fig. 12b it is possible to observe that the periodicity failures regard cases in which the fragment orbit

semi-major axis and eccentricity are very close to the parent values. Indeed, in this situation, the two orbits have a similar period and shape, and, from a i-th periodicity to the following one, there is not a remarkable difference in the relative distance distribution R (the MOID distribution M is always the same, being the scenario Keplerian). This weakens the statistical comparison result, as the EMD is similar across multiple clusters, and the algorithm possibly converges to an erroneous solution. Instead, from Fig. 12c and Fig. 12d it is worth to notice that both compliant and uncompliant MOID failures regard cases in which fragment and parent inclination and right ascension of the ascending node are very close each other, as the similar orientation provokes a remarkable excursion of MOID data from a sample to another, and the samples cluster around a quantity corresponding to an epoch which is not the correct value. Overall, this practically confirms the two theoretical sources of failure mentioned in Section 1.

A detailed computational demand study is not carried out, given the current prototype implementation in MATLAB (MATLAB, 2020), but it can be quantified in about 30 s per fragment by using a single core with the same Intel(R) Core(TM) i7-8700 CPU @ 3.20 GHz - 3.19 GHz processor. This low computational demand is linked to the analytical propagation exploited in the unperturbed scenario.

Sensitivity analysis on the number of samples used

As described in Section 2, FRED algorithm starts from the IOD result (expressed in terms of mean state and covariance), and populate it by samples according to a multi-normal distribution. Thus, the larger the number of samples used, the more accurate the IOD uncertainty representation. The number of samples used is a key point in assessing FRED performance and, for this reason, a sensitivity analysis is here conducted by modifying the nominal value of $N_s = 1000$ to 100, 500, 2000 and 10000. It must be pointed out that the larger the number of samples used, the larger the computational demand, as more conjunctions for each fragment are to be computed (both in terms of MOID and relative distance evaluation). In addition, also the computational demand of the EMD metrics is proportional to the number of samples.

The results are reported in Table 3. It is possible to notice that the performance are stable across the different values of N_s, and remain similar to the EMD metrics results reported in Table 2. In particular, it is to point out that the convergence rate to the correct solution does not improve for a larger number of samples used in a monotonic way. This confirms that the failure cases are not related to an uncertainty representation which is not dense enough, but to the mutual geometry between parent and fragment orbits, as discussed above regarding Fig. 12. On the one hand, this is an important result, as the method computational demand can be reduced by using a lower

(a) Semi-major axis.

(b) Eccentricity.

(c) Inclination.

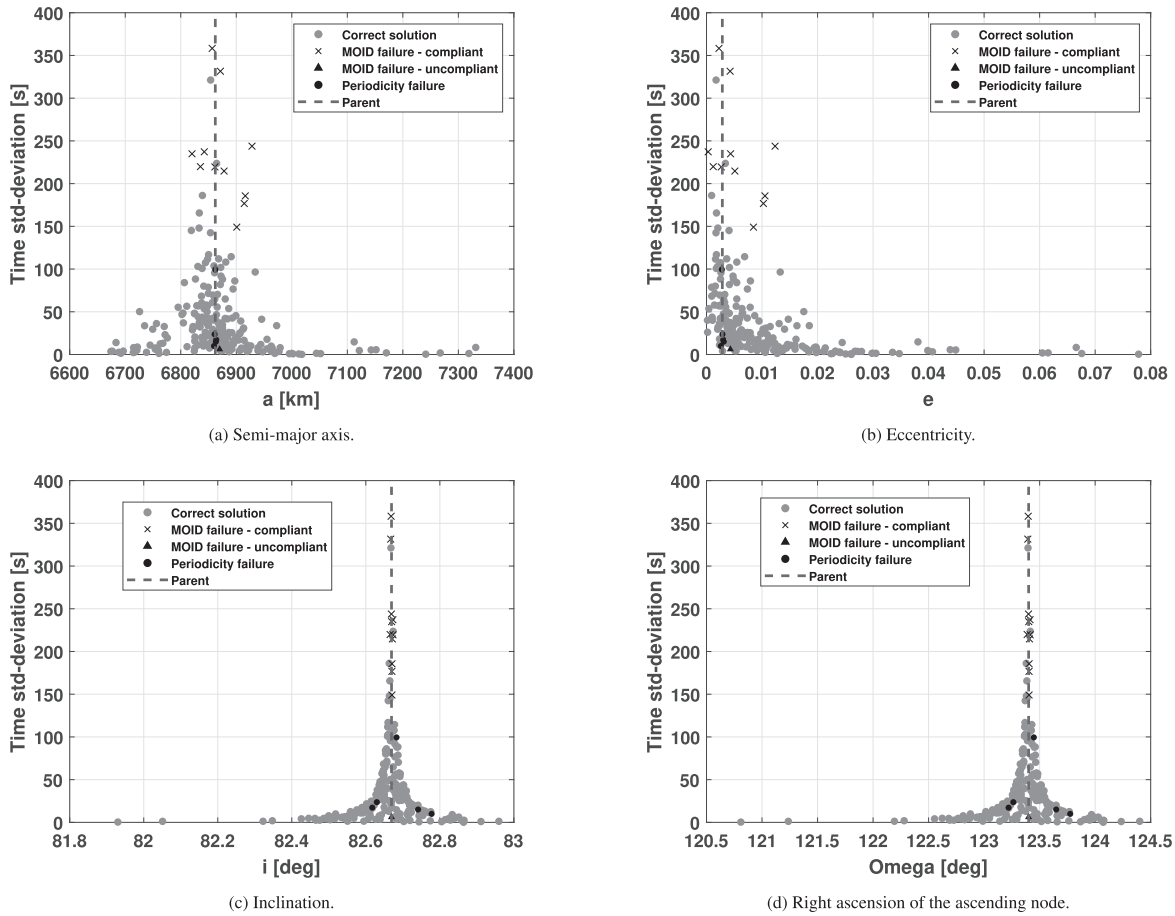(d) Right ascension of the ascending node.

Fig. 12. Unperturbed scenario: relationship between the standard deviation associated to the computed fragmentation epoch and the fragment semi-major axis, eccentricity, inclination and the right ascension of the ascending node. The fragments for which a failure occurs are highlighted according to the legend, and the dashed line shows the parent orbital parameters.

Table 3
Unperturbed scenario: sensitivity analysis on the number of samples used.

	Correct solutions	MOID failures compliant	MOID failures uncompliant	Periodicity failures
100	92.4%	3.9%	0.4%	3.4%
500	92.0%	4.2%	0.4%	3.4%
2000	92.4%	4.2%	0.4%	3.0%
10000	92.8%	4.2%	0.4%	2.6%

number of samples, without a performance degradation. On the other hand, the larger the number of samples, the better the representation of the IOD uncertainty. Therefore, a trade-off choice must be conducted. For these reasons, the nominal value of $N_s = 1000$ samples is kept in the following analyses.

3.3. Perturbed scenario with no IOD error

The same analysis as above is conducted on a perturbed scenario in which SGP4 (Vallado et al., 2006) is used both to derive the fragments actual trajectory, and in FRED algorithm. The data set is created as follows:

1. The last available TLE of the parent object is propagated up to the fragmentation epoch, which is always set at 02:47:00 UTC of November 15th, 2021, and converted in Cartesian coordinates.
2. The fragmentation impulses are applied, again according to the NASA standard break-up model (NASA, 2011).
3. Each fragment state is converted in SGP4 elements through a fixed-point iteration loop based on a Non-linear Least Squares (Coleman and Li, 1996). In particular, the B*, which accounts for the physical characteristics of the object, is computed by:

(a) Propagating the fragment orbital state through the high-fidelity propagator described in (Cipollone et al., 2022). To this end, the ballistic coefficient was provided by the NASA break-up model.

(b) Searching for the B* which allows the SGP4 propagation to best match the high-fidelity propagation, through a Non-linear Least Squares filter. Out of the 237 fragments of the original data set, for 28 the process does not converge to a solution. Thus, a data set of 209 fragments is considered from now on.

The computed B* distribution is reported in Fig. 13a.

4. Similarly to the analysis in Section 3.2, each fragment elements are propagated through SGP4 for 13 h, when the observation is simulated by computing the fragment orbital state in Cartesian coordinates and associating the same covariance used in Section 3.2.

Then, in FRED algorithm, each fragment sample is propagated through SGP4. This operation implies a first conversion from Cartesian coordinates to SGP4 elements (at the IOD epoch), and then from SGP4 elements to Cartesian coordinates at the end of the propagation (that is at the epochs t_i defined in Section 2) to compute the MOID and the relative distance.

Both in data set generation and inside FRED algorithm, the conversion from Cartesian coordinates to SGP4 elements introduces an error which, although negligible at the considered epoch, increases with the propagation and may affect results at the epochs t_i. On the contrary, the presence of perturbations in the propagation introduces an additional difference among clusters, besides the one related to the phasing effect between parent and fragment samples orbital states. This can be observed in Fig. 13b, which reports the clusters in the plane time of transit of parent through the MOID versus MOID magnitude, for the same case as the one reported in Fig. 4a for the Keplerian scenario. Comparing the two figures, it can be appreciated how the perturbations introduce a difference among the clusters.

FRED results for the perturbed scenario are reported in Table 4 considering the Earth Mover Distance metrics, and represented in Fig. 14. A deterioration in performance may be noticed, due to the fact that the number of fragments in data set decreases, as mentioned above, and both the uncompliant MOID and the periodicity failures increase, passing from 1 and 5 to 2 and 8 respectively. Similarly to Fig. 11, Fig. 14 confirms that FRED algorithm is more prone to fail for those fragments originated by a small impulse magnitude.

As in Section 3.2, it is interesting to study the relationship between the time standard deviation associated to the solution and the orbital parameters, as represented in Fig. 15. All the considerations as in Section 3.2 are valid, to testify that the most failure prone situations (similar orbital period and orientation) do not change when perturbations are considered in the dynamics.

The computational demand increases with respect to the unperturbed scenario (under the same conditions), resulting in about 5 min per fragment analysed. This is due both to SGP4, which requires more computational time than the unperturbed analytical propagation, and to the fact that, for each *j*-th fragment sample, the MOID data are recursively refined until the flying time to the MOID falls below 1e-03 s (as described in Section 2).

To assess the general applicability of FRED algorithm, the same simulation as in Section 3.3 is reported in Appendix considering a Medium Earth Orbit (MEO) and a Geostationary Orbit (GEO) fragmentation.

3.4. Perturbed scenario with IOD error

The analyses in Section 3.2 and Section 3.3 are conducted with no error associated to IOD, that is starting from an orbital state obtained by simply propagating the fragment nominal ephemeris up to a certain epoch, considering it as the mean state and associating a covariance to it. However, in real applications, at the orbit determination epoch a mismatching between the orbital state mean and
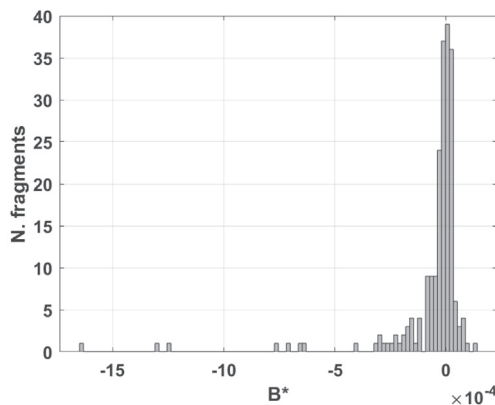
(a) B* distribution from the matching between SGP4 and the high-fidelity propagation.
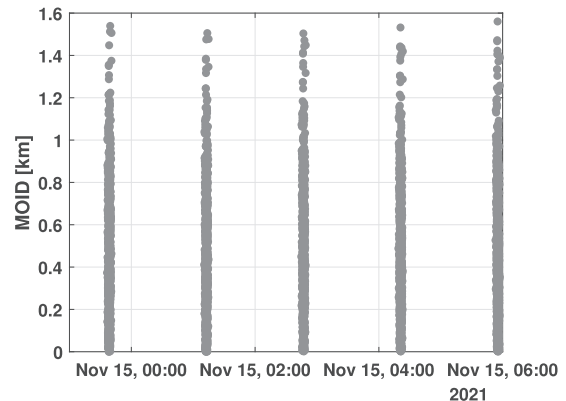
(b) Distribution of the t_j^p epochs in the time window of the analysis.

Fig. 13. B* distribution and FRED clusters in the perturbed scenario.

Table 4
Perturbed scenario results for EMD metrics.

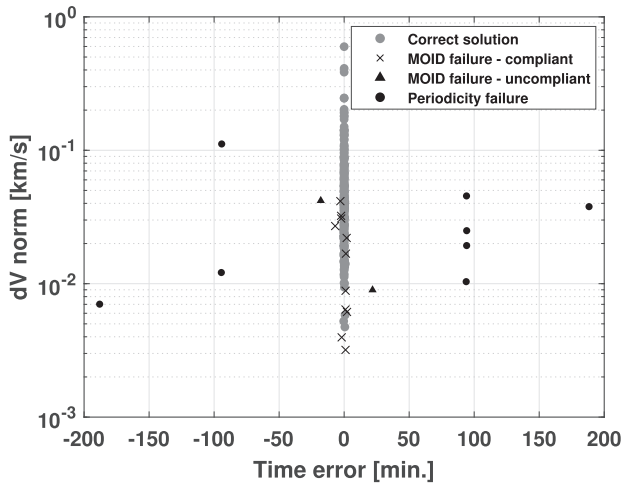| Correct solutions	MOID failures compliant	MOID failures uncompliant	Periodicity failures
90.0%	5.3%	0.9%	3.8%

Fig. 14. Results of the numerical analysis on the perturbed scenario with no orbital state error. The graph represents, for each fragment analysed, the relationship between the magnitude of the impulse which generated it (in logarithmic scale) and the time error between the estimated and the correct fragmentation epochs. The fragments for which a failure occurs are highlighted according to the legend.

the ground truth is introduced by the IOD process, and its effects on FRED algorithm must be assessed.

For this purpose, an analysis is carried out by starting from an orbital state generated through a surveillance radar observation, which allows to run a IOD from the measurements acquired during a single observation, also if this lasts few tens of seconds (Bianchi et al., 2022).

- The ground truth of the fragment orbital state is generated in the same manner as in Section 3.3, that is propagating the fragment ephemeris for 13 h from the event through SGP4 (Vallado et al., 2006) and with the estimated B*.
- Geodetic latitude and longitude are computed from the fragment position, and a monostatic radar station is simulated at 0 km altitude and with a small variation of +1 deg from the fragment coordinates. Such a variation prevents the target from exactly transiting through the station zenith direction.
- Azimuth, elevation and slant range are simulated for the following 30 s. A Gaussian noise is added of 0.01 deg (on angular coordinates) and 30 m (on slant range), coherently with the real data analyses presented in (Montaruli et al., 2022a).
- The orbital state is computed at the initial observation epoch, through the IOD procedure presented in (Siminski, 2016), which computes the orbital state at

the first observation epoch through an unperturbed analytic propagation. By this way, a dynamical model error is included in the IOD process, as the measurements were simulated through a propagation based on SGP4. No further refinement is done in the simulations, to test the procedure for a coarse IOD result.

In this way, the fragment orbital state $\{x^{fg}, P^{fg}\}$ is obtained, and FRED algorithm is run. It is worth to stress that an error between x^{fg} and the fragment actual position and velocity is now present, and the covariance P^{fg} is computed from the measurements through the IOD procedure, that is differently from what done in Section 3.2 and in Section 3.3.

Results are reported in Table 5 and represented in Fig. 16. It is worth to observe that in most cases the algorithm converges to the correct solution. However, comparing Table 5 to Table 2 and Table 4, it can be noticed that the IOD mismatching remarkably affects the algorithm performance, especially for what concerns the metrics to select the correct candidate. This can be visualised also by comparing Fig. 16 with Fig. 11 and Fig. 14.

Concerning the relationship between the time standard deviation associated to the solution and the orbital parameters, represented in Fig. 17, it may be noticed that the more similar the fragment and the parent orbits are, the larger the time uncertainty associated to the FRED solution, as already discussed about Fig. 12 and Fig. 15. This relationship is more evident for the inclination (Fig. 17c) and and the right ascension of the ascending node (Fig. 17d). The relationships between orbital parameters and failures are analogous to those in Fig. 12 and Fig. 15, but they are less clear because of the orbit determination error.

Overall, the computational time is similar to the one in Section 3.3.

To further appreciate FRED results, an alternative analysis, analogous to the method described at the beginning of Section 2, is carried out. Such an approach assesses the fragmentation epoch as the time of the minimum relative distance between parent and fragment mean states (both assumed as deterministic), propagated on the analysis time window. This would allow a lower computational demand. The results are reported in Table 6, where a much smaller convergence to the correct solution can be observed. Therefore, besides providing statistical information and the correct solution among fragmentation epoch candidates, FRED convergence to the correct solution turns out to be more robust.

(a) Semi-major axis.

(b) Eccentricity.

(c) Inclination.
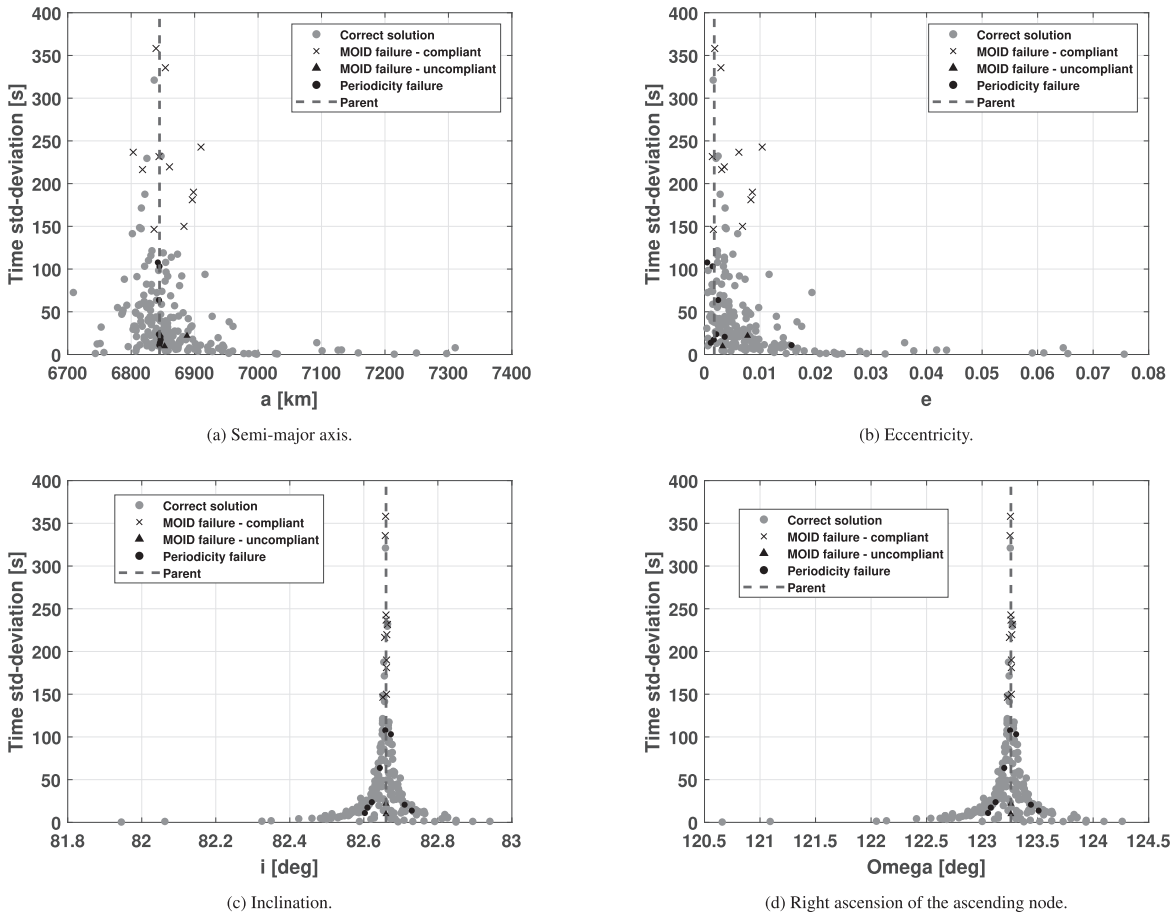

(d) Right ascension of the ascending node.

Fig. 15. Perturbed scenario: relationship between the standard deviation associated to the computed fragmentation epoch and the fragment semi-major axis, eccentricity, inclination and right ascension of the ascending node. The fragments for which a failure occurs are highlighted according to the legend, and the dashed line shows the parent orbital parameters.

Table 5
Results for the perturbed scenario and accounting for the orbital state error introduced by the IOD process. The EMD metrics is used.

Correct solutions	MOID failures compliant	MOID failures uncompliant	Periodicity failures
68.9%	9.6%	0.5%	21.0%

3.5. Sensitivity analysis

A sensitivity analysis regarding the scenario in Section 3.4 is conducted to test FRED robustness. Operationally, three aspects may negatively affect the results:

- A larger time elapsed between the event and the IOD: given the IOD error, the larger the propagation time, the larger the mismatching at the fragmentation epoch.
- A wrong evaluation of the physical parameter of the fragment: the physical characteristics of the fragment can be either assumed or reconstructed during the IOD process, and this likely create an additional source of mismatching.
- A larger measurements noise: this generally induces a more noisy IOD result, with larger mismatching between IOD mean state and larger covariance.

For all these aspects a sensitivity analysis is carried out as follows, by also comparing the FRED results with the ones obtained through the relative distance metrics introduced in Section 3.4.

3.5.1. Sensitivity Analysis on the IOD epoch

In Section 3.2, Section 3.3 and Section 3.4, the IOD epoch is always set 13 h after the event, as FRED algorithm aims at providing a method to identify the fragmentation epoch from a fragment orbital state determined in the first hours right after the event. However, in real case scenarios, the algorithm may need to be applied starting from an orbital state resulting from an IOD conducted later. For this reason, it is fundamental to assess the FRED performance by considering larger time elapsed between the fragmentation and the IOD epochs. Three cases are
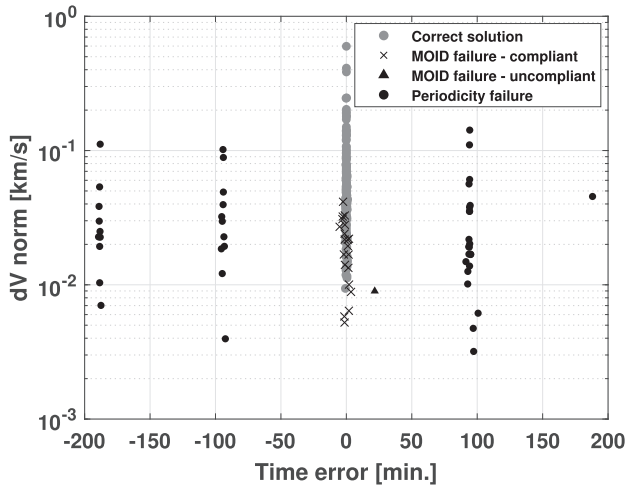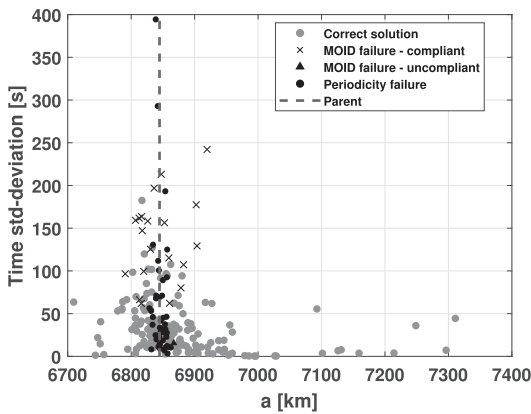
Fig. 16. Results for the perturbed scenario and accounting for the orbital state error introduced by the IOD process. The graph represents, for each fragment analysed, the relationship between the magnitude of the impulse which generated it (in logarithmic scale) and the time error between the estimated and the correct fragmentation epochs. The fragments for which a failure occurs are highlighted according to the legend.

investigated: 24 h, 48 h and 72 h from the event to the first observation epoch. As above, the IOD method presented in (Siminski, 2016) is applied. Results are reported in Table 7 and show a deterioration in performance, and this confirms that the longer the time elapsed, the less robust the algorithm is. Furthermore, a longer time elapsed implies a longer fragment samples propagation, which increases the computational cost.

The FRED results are compared to those which could be obtained with the deterministic relative distance metrics, which are reported in Table 8. There is an oscillating behaviour of the correct solution, but the general trend confirms that the longer the time elapsed, the less performing the deterministic metrics. Moreover, the results are always much worse than the FRED ones.
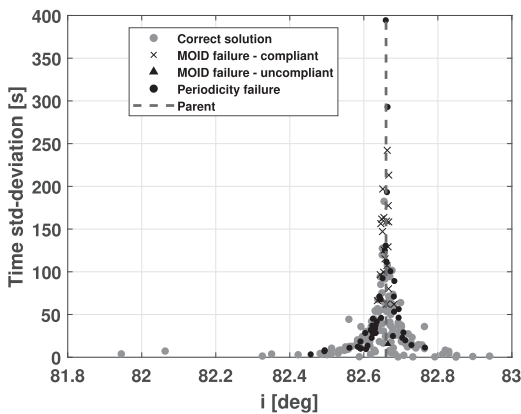
3.5.2. Sensitivity Analysis on the B* mismatching
In the above analyses, the same B* (expressing the physical parameter in the SGP4 propagator (Vallado et al., 2006)) is used to generate the ground truth and inside FRED algorithm. This is a strong assumption, as opera-
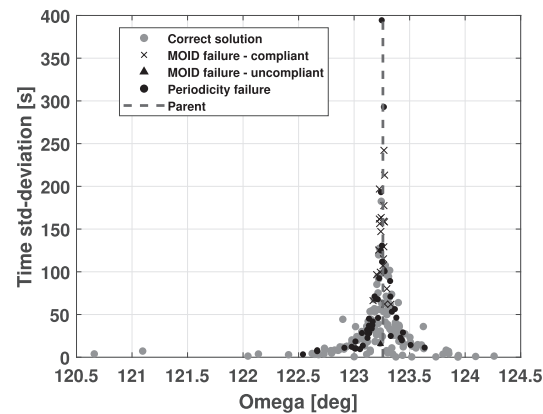

(a) Semi-major axis.
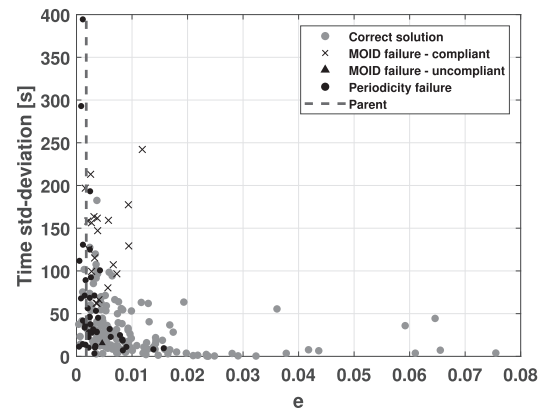
(b) Eccentricity.

(c) Inclination.

(d) Right ascension of the ascending node.

Fig. 17. Perturbed scenario and accounting for the orbital state error introduced by the IOD process: relationship between the standard deviation associated to the computed fragmentation epoch and the fragment semi-major axis, eccentricity, inclination and right ascension of the ascending node. The fragments for which a failure occurs are highlighted according to the legend, and the dashed line shows the parent orbital parameters.

Table 6
Results for the perturbed scenario and accounting for the orbital state error introduced by the IOD process. A deterministic metrics is used, according to which the fragmentation epoch is assessed as the time of the minimum relative distance between the parent and the fragment mean state (both assumed as deterministic), propagated on the analysis time window.

	Correct solutions	1 min $< t_{err} < T^p/2$	$t_{err} > T^p/2$
Relative distance	12.4%	67.0%	20.6%

Table 7
Perturbed scenario with orbital state error introduced by the IOD process: FRED results for the sensitivity analysis on the time elapsed between the fragmentation and the IOD epoch.

Time from the event	Correct solutions	MOID failures compliant	MOID failures uncompliant	Periodicity failures
24 h	60.8%	5.7%	0.0%	33.5%
48 h	43.1%	3.8%	1.0%	52.1%
72 h	31.6%	2.4%	0.5%	65.5%

Table 8
Perturbed scenario with orbital state error introduced by the IOD process: deterministic relative distance metrics results for the sensitivity analysis on the time elapsed between the fragmentation and the IOD epoch.

Time from the event	Correct solutions	1 min $< t_{err} < T^p/2$	$t_{err} > T^p/2$
24 h	8.1%	57.9%	34.0%
48 h	3.4%	42.1%	54.5%
72 h	4.3%	31.6%	64.1%

tionally no physical information about the observed fragment is known. Generally, during an OD process, the physical parameters can be estimated as well, but accurate measurements are needed, as well as a long observation arc (possibly obtained by linking more measurements tracks). This is not the case for a single observation right after a fragmentation event, and the physical parameters are either roughly estimated or not estimated at all and, so, assumed. In addition, the IOD procedure used (Siminski, 2016) estimates the orbital state only, which is voluntarily not refined through additional filters, as stated in Section 3.4.

To test FRED algorithm robustness to the physical parameter mismatching, a sensitivity analysis is carried out considering, inside the FRED algorithm, B* values different from the one used to generate the ground truth. This modification is obtained by multiplying the correct B* times: 1e+01, 1e-01, 1e-02, 1e-03, 0.

The results are reported in Table 9. FRED performance turns out to be robust to erroneous physical parameter estimation, and, for the 1e+01, the 1e-01, the 1e-03 and the 0 cases, the percentages are exactly the same as the nominal scenario ones (Table 5). Moreover, in the 1e-02 case the result for one fragment passes from being a compliant

MOID failure to a correct solution. Overall, these results cannot be considered as a general behaviour, as the algorithm sensitivity on the physical parameters always depends on the perturbations experienced by the fragment and, so, on its orbital regimen. This is even more true considering the short propagation period of the simulation. For the scenario analysed, also the distribution of the relative distance metrics result does not change, as visible in Table 10.

3.5.3. Sensitivity analysis on the measurements noise

As mentioned above, the performance of FRED algorithm in operational scenarios strongly depends on the IOD accuracy, which in turn depends on the algorithm used, the observation geometry and length, and on the measurements quality. Indeed, the deterioration of measurements can lead to two effects on the IOD result and, so, on FRED performance: an erroneous orbital mean state and a larger uncertainty. For this reason, it is fundamental to assess FRED algorithm sensitivity to the measurements noise. In particular, since in surveillance radars (the on-ground sensors of the nominal analysis) the angular track is the less accurate measurement, the noise associated to the range is kept fixed to the nominal value of 30 m,

Table 9
Perturbed scenario with orbital state error introduced by the IOD process: FRED results for the sensitivity analysis on the B*.

Factor multiplying B*	Correct solutions	MOID failures compliant	MOID failures uncompliant	Periodicity failures
1e+01	68.9%	9.6%	0.5%	21.0%
1e-01	68.9%	9.6%	0.5%	21.0%
1e-02	69.4%	9.1%	0.5%	21.0%
1e-03	68.9%	9.6%	0.5%	21.0%
0	68.9%	9.6%	0.5%	21.0%

Table 10
Perturbed scenario with orbital state error introduced by the IOD process: deterministic relative distance metrics results for the sensitivity analysis on the B*.

Factor multiplying B*	Correct solutions	$1\ min < t_{err} < T^p/2$	$t_{err} > T^p/2$
1e+01	12.4%	67.0%	20.6%
1e-01	12.4%	67.0%	20.6%
1e-02	12.4%	67.0%	20.6%
1e-03	12.4%	67.0%	20.6%
0	12.4%	67.0%	20.6%

while the angular noise is made varying from the nominal value of 1e-02 deg to: 2e-02 deg, 5e-02 deg and 1e-01 deg.

The results are reported in Table 11. It is possible to notice that the larger the noise associated to the angular track, the lower the convergence to the correct solution and the larger the periodicity failures percentage. There is a slight increase also in the MOID compliant failures, while the uncompliant ones tend to zero. These results depend on the IOD result deterioration, which introduces a mismatching affecting the estimation of MOID data. On the one hand this may lead to a wrong evaluation through the EMD metrics, with still the correct epoch among candidates. On the other hand the IOD result may induce a wrong computation of time of parent transit through the MOID and, so, the epoch candidates may be wrongly estimated, and this may result in the absence of the correct solution among candidates. In any case, FRED is always better performing than the relative distance metrics, whose results are reported in Table 12. Also in this case there is a performance deterioration with the angular noise increase.

4. Conclusions

The paper described FRED algorithm, which deals with the fragmentation epoch identification problem focusing on the case in which, besides the last available ephemeris of the parent object (assumed as a deterministic quantity), just one single fragment stochastic orbital state is available and already linked to the event. The algorithm computes the fragmentation epoch candidates, which are ranked according to the matching between MOID and relative distance distributions, given that, at the actual fragmentation epoch, the MOID and the relative distance were equal. To compute the statistical matching, three metrics are discussed: the Mahalanobis distance, a tailored procedure based on the quantiles coupled with a Principal Component Analysis and the Earth Mover's Distance. The latter is eventually selected as the most performing and the most

suitable for the problem, given the non-Gaussian distributions involved.

The numerical simulations highlighted that the algorithm reliability decreases when the observed fragment orbit has either the period or the orbital plane similar to the parent object one, and a sensitivity analysis showed that there is no remarkable dependence on the number of samples used in representing the fragment orbital state. The inclusion of the perturbations and, moreover, of the orbit determination error deteriorates the performance, but the correct fragmentation epoch can still be identified among candidates. In addition the algorithm always features much better results with respect to an alternative deterministic metrics based on the minimum relative distance between the parent ephemeris and the fragment mean state propagated on the analysis time window. A further sensitivity analysis shows a deterioration proportional to the angular noise associated to the solution and to the time elapsed between the event and the observation, but FRED is always much more performing than the relative distance metrics. Instead, no remarkable change occurs considering a mismatching between the actual value of the fragment physical parameter and the one used in the algorithm, but this depends on the fragment orbital regimen and on the elapsed time from the event to the observation, and so it is not possible to consider it as a general result.

In operational applications, FRED performance may be improved through multiple sensors contributions and by refining the fragment orbital state with a smarter orbit determination process (Montaruli et al., 2022b), by possibly exploiting the parent orbital state prediction as first guess for those fragments generated by small magnitude impulses. Furthermore, the plausibility of FRED fragmentation epoch candidates can be examined by tasking the sensors to point at the right ascensions and declinations where the parent was at those epochs and retain only candidates featuring a sufficient number of fragments detected. This action cannot be decisive, as periodicity failures may share the same right ascension and declination as the

Table 11
Perturbed scenario with orbital state error introduced by the IOD process: FRED results for the sensitivity analysis on the angular track noise.

Angular noise [deg]	Correct solutions	MOID failures compliant	MOID failures uncompliant	Periodicity failures
2e-02	66.5%	11.5%	0.5%	21.5%
5e-02	53.1%	20.6%	0.0%	26.3%
1e-01	33.5%	29.7%	0.0%	36.8%

Table 12
Perturbed scenario with orbital state error introduced by the IOD process: deterministic relative distance metrics results for the sensitivity analysis on the angular track noise.

Angular noise [deg]	Correct solutions	$1\ \text{min} < t_{err} < T^p/2$	$t_{err} > T^p/2$
2e-02	13.4%	57.4%	29.2%
5e-02	12.0%	59.8%	28.2%
1e-01	11.5%	57.9%	30.6%

correct solution, but it can support to shrink the candidates set. Finally, the parallel use of FRED algorithm on different fragments would allow to reach a higher level of confidence and precision in the provided results, both in terms of the epoch candidates set and of the one eventually returned by the algorithm. This could be beneficial when multiple fragments are detected and associated to the event, and they provide an orbit determination result, but they are too few to be used in the deterministic approaches mentioned in Section 1.

Concerning possible upgrades, the multivariate normal distribution used represents the most generic approach, but an alternative and less computational demanding way of covariance propagation may be integrated in the process. In addition, the algorithm considers the last available ephemeris as a deterministic information, while an uncertainty is associated also to it and may be included in the overall process. Another aspect which may be further studied is the fragmentation epoch candidates ranking strategy, which is currently performed based on the statistical matching between the relative distance and the MOID distributions, but which may profit from other conjunction analysis tools, like the long-term risk assessment. Finally, it would be interesting to deal with the fragmentation epoch identification problem in the case that it is not possible to determine the fragment orbital state, with a tailored procedure conducted in the measurements space. To this end, developing an approach to solve a track to track

association problem to link multiple measurements referred to a same fragment would allow to derive an orbit determination result and to exploit FRED algorithm. Overall, all these possible algorithm improvements and developments should be carried out together with test on real data and the final operational implementation shall include a detailed computational demand assessment and minimisation.

Declaration of Competing Interest

The authors declare that they have no known competing financial interests or personal relationships that could have appeared to influence the work reported in this paper.

Acknowledgement

Table 13
COSMOS 1490 and EDRS-C orbital parameters simulated on November 15th 2022, at 02:47:00 UTC.

	a [km]	e	i [deg]	Ω [deg]	ω [deg]	θ [deg]
COSMOS 1490	2.6e+04	1.5e-03	64.2	130.2	18.9	182.1
EDRS-C	4.2e+04	6.2e-05	0.0	89.9	165.5	104.3

Table 14
Epochs of COSMOS 1490 and EDRS-C last available ephemerides and event alert

	Last available ephemeris epoch (UTC)	Event alert epoch (UTC)	Orbit determination epoch (UTC)
COSMOS 1490	November 14th, 02:07:03	November 16th, 00:00:00	November 16th, 07:35:00
EDRS-C	November 12th, 18:26:49	November 18th, 06:00:00	November 18th, 10:00:20

Table 15
FRED results for the COSMOS 1490 and EDRS-C simulated fragmentations. The perturbed scenario with no orbital state error is assessed, and the EMD metrics is used.

	Correct solutions	MOID failures compliant	MOID failures uncompliant	Periodicity failures
COSMOS 1490	89.9%	9.1%	0.0%	1.0%
EDRS-C	86.5%	11.5%	0.5%	1.9%

Appendix A.

The same analysis as in Section 3.3, that is a perturbed scenario with no IOD error, is here conducted simulating the fragmentations of two objects: the COSMOS 1490, flying in Medium Earth Orbit (MEO), and the EDRS-C, flying in geostationary orbit (GEO). Analogously to Section 3.1, the fragmentation event is simulated at 02:47:00 UTC of November 15th, 2021, and modelled through the same set of impulses. The orbital parameters of the two parent objects at the break-up epoch are reported in Table 13.

The epochs of the last available ephemeris, of the considered event alert and of the orbit determination result are reported in Table 14. These epochs were selected to set an analysis time window which includes the same number of periodicities as the one in Section 3. Similarly to Section 3.3, at the orbit determination epoch a covariance is associated, with inertial position and velocity standard deviations of 1.4e+00 km and 2.5e-04 km/s, for the COSMOS 1490, and 3.1e+00 km and 4.9e-04 km/s, for the EDRS-C. These quantities were derived from an orbit determination process.

The results are reported in Table 15. It can be noticed that both for COSMOS 1490 and EDRS-C the convergence to the correct solution is similar to the one in Section 3.3. The increase in compliant MOID failures is motivated by the larger propagation time window, which makes the samples more spread, resulting in possible wrong fragmentation epoch estimates provided with a time error smaller than the associated uncertainty. Overall, this analysis confirms FRED general applicability, as the algorithm behaviour does not depend on the orbital regimen of the fragmentation event.

References

Andrisan, R.L., Ionita, A., González, R.D. et al., 2016. Fragmentation event model and assessment tool (fremat) supporting on-orbit fragmentation analysis. In: 7th European Conference on Space Debris.

Bianchi, G., Montaruli, M.F., Roma, M. et al., 2022. A new concept of transmitting antenna on bi-static radar for space debris monitoring. In: International Conference on Electrical, Computer, Communications and Mechatronics Engineering, ICECCME 2022. URL: www.scopus.com.

Cipollone, R., Montaruli, M.F., Faraco, N. et al., 2022. A re-entry analysis software module for space surveillance and tracking operations. In: International Astronautical Congress: IAC Proceedings, pp. 1–7.

Coleman, T.F., Li, Y., 1996. An interior trust region approach for nonlinear minimization subject to bounds. SIAM J. Optim. 6 (2), 418–445. https://doi.org/10.1137/0806023, arXiv:https://doi.org/10.1137/0806023.

Di Mare, L., Cicalò, S., Rossi, A. et al., 2019. In-orbit fragmentation characterization and parent bodies identification by means of orbital distances. In: First International Orbital Debris Conference, volume 2109 of LPI Contributions, p. 6007.

ESA, 2023. Space debris by the numbers. Available online at: https://www.esa.int/Space_Safety/Space_Debris/Space_debris_by_the_numbers, Last accessed January 16th, 2023.

Ester, M., Kriegel, H.-P., Sander, J. et al., 1996. A density-based algorithm for discovering clusters in large spatial databases with noise. In: Proceedings of the Second International Conference on Knowledge Discovery and Data Mining KDD'96, AAAI Press, p. 226–231.

European Space Surveillance and Tracking, 2021. EUSST Service Portfolio.

EUSST, 2021. Cosmos 1408 fragmentation. Available online at: https://www.eusst.eu/newsroom/eu-sst-confirms-fragmentation-cosmos-1408/, Last accessed August 18th, 2022.

Frey, S., Colombo, C., Lemmens, S., 2018. Density based modelling and indication of break-up location and epoch from fragments using backwards propagation. In: 5thEuropean Workshop on Space Debris Modelling and Remediation.

Gronchi, G.F., 2005. An algebraic method to compute the critical points of the distance function between two keplerian orbits. J. Celestial Mech. Dyn. Astron. 93 (1), 295–329.

Hoots, F.R., Crawford, L.L., Roehrich, R.L., 1984. An analytic method to determine future close approaches between satellites. J. Celestial Mech. Dyn. Astron. 33 (2), 143–158.

Hoots, F.R., Roehrich, R.L., 1980. Spacetrack Report No. 3: Models for propagation of NORAD element sets. Technical Report Aerospace Defense Center, Peterson Air Force Base.

IADC, 2002. Inter-Agency Space Debris Coordination Committee - Space Debris Mitigation Guidelines.

Jolliffe, I., 2011. Principal component analysis. In: Lovric, M. (Ed.), International Encyclopedia of Statistical Science, Springer, Berlin Heidelberg, Berlin, Heidelberg, pp. 1094–1096, https://doi.org/10.1007/978-3-642-04898-2_455.

Kessler, D.J., Cour-Palais, B.G., 1978. Collision frequency of artificial satellites: The creation of a debris belt. J. Geophys. Res., 2637–2646

Kotz, S., Balakrishnan, N., Johnson, N.L., 2000. Continuous Multivariate Distributions. Models and Applications volume Volume 1: Models and Applications, 2nd ed., John Wiley, New York.

Letizia, F., Colombo, C., Lewis, H.G., 2015. Analytical model for the propagation of small-debris-object clouds after fragmentations. J. Guidance Control Dyn. 7¹'38 (8), 1478–1491.

Letizia, F., Colombo, C., Lewis, H.G., 2016. Multidimensional extension of the continuity equation method for debris clouds evolution. Adv. Space Res. 57 (8), 1624–1640.

Levina, E., Bickel, P., 2001. The earth mover's distance is the mallows distance: some insights from statistics. In: Proceedings Eighth IEEE International Conference on Computer Vision. ICCV 2001, vol. 2, pp. 251–256. https://doi.org/10.1109/ICCV.2001.937632.

Mahalanobis, P.C., 1936. On the generalized distance in statistics. Proc. Nat. Inst. Sci. (Calcutta), 2, 49–55.

MATLAB, 2020. 9.9.0.1538559 (R2020b). Natick, Massachusetts: The MathWorks Inc.

McKnight, D., Witner, R., Letizia, F., et al., 2021. Identifying the 50 statistically-most-concerning derelict objects in leo. Acta Astronaut. 181, 282–291. https://doi.org/10.1016/j.actaastro.2021.01.021, URL: https://www.sciencedirect.com/science/article/pii/S0094576521000217.

Montaruli, M.F., Facchini, L., Lizia, P.D., et al., 2022a. Adaptive track estimation on a radar array system for space surveillance. Acta Astronaut. https://doi.org/10.1016/j.actaastro.2022.05.051, URL: https://www.sciencedirect.com/science/article/pii/S0094576522002703.

Montaruli, M.F., Purpura, G., Cipollone, R. et al. (2022b). A software suite for orbit determination in space surveillance and tracking applications. In 9th European Conference for Aerospace Sciences (EUCASS 2022) (pp. 1–12).

Muciaccia, A., Facchini, L., Montaruli, M.F. et al., 2022. Observation and analysis of cosmos 1408 fragmentation. In: International Astronautical Congress: IAC Proceedings, pp. 1–7.

NASA, 2011. Proper implementation of the 1998 nasa breakup model. Orbital Debris Quarterly News 15 (4), 4–5.

Romano, M., Muciaccia, A., Trisolini, M. et al., 2021. Characterising in-orbit fragmentations with the puzzle software. In: 8th International Conference on Astrodynamics Tools and Techniques (ICATT).

SciPy, 2022. Scipy documentation. Available online at: https://docs.scipy.org/doc/scipy/, Last accessed August 18ᵗʰ, 2022.

Siminski, J., 2016. Techniques for assessing space object cataloguing performance during design of surveillance systems. In: 6th International Conference on Astrodynamics Tools and Techniques (ICATT), pp. 14–17.

Space-track, 2022. Space-track website. Accessed 16.01.2023, https://www.space-track.org/auth/login.

Vallado, D., Alfano, S., 2014. Curvilinear coordinate transformations for relative motion. Celestial Mech. Dyn. Astron. 118. https://doi.org/10.1007/s10569-014-9531-1.

Vallado, D.A., Crawford, P., Hujsak, R. et al., 2006. Revisiting Spacetrack Report #3. In: AIAA Astrodynamics Specialists Conference and Exhibit.